ON A PERIODICALLY FORCED, WEAKLY DAMPED PENDULUM. PART 1: APPLIED TORQUE

PETER J. BRYANT[1] AND JOHN W. MILES[2]

Abstract

Coplanar forced oscillations of a mechanical system such as a seismometer or a fluid in a tank are modelled by the coplanar motion of periodically forced, weakly damped pendulum. We consider the phase-locked solutions of the differential equation governing planar motion of a weakly damped pendulum driven by a periodic torque. Sinusoidal approximations previously obtained for downward and inverted oscillations at small values of the dimensionless driving amplitude ε are continued into numerical solutions at larger values of ε. Resonance curves and stability boundaries are presented for downward and inverted oscillations of periods T, $2T$, and $4T$, where $T(\equiv 2\pi/\omega)$ is the dimensionless forcing period. The symmetry-breaking, period-doubling sequences of oscillatory motion are found to occur in bands on the (ω, ε) plane, with the amplitudes of stable oscillations in one band differing by multiples of about π from those in the other bands, a structure similar to that of energy levels in wave mechanics. The sinusoidal approximations for symmetric T-periodic oscillations prove to be surprisingly accurate at the larger values of ε, the banded structure being related to the periodicity of the J_0 Bessel function.

1. Introduction

We consider a pendulum of length l driven by a torque $\varepsilon g l \sin \omega t$ per unit mass applied about its pivot. The equation of motion is

$$\ddot{\theta} + 2\delta\dot{\theta} + \sin\theta = \varepsilon \sin \omega t, \tag{1.1}$$

where θ is the angular displacement from the downward vertical, δ is the damping ratio (actual/critical), ω is the ratio of the forcing frequency

[1]Department of Mathematics, University of Canterbury, Christchurch, New Zealand.
[2]Institute of Geophysics and Planetary Physics, University of California at San Diego, La Jolla, California 92093, U.S.A.

1

to the natural frequency, and the unit of time is the inverse natural frequency. Periodic solutions of (1.1) describing oscillations about the downward vertical have been obtained by Miles [6] on the alternate hypotheses that (i) the contributions of the second and higher harmonics to the oscillatory motion are negligible or (ii) the solution is close to that for free oscillations. Miles [8] also calculated periodic solutions describing oscillations about the upward vertical based on hypothesis (i). Neither hypothesis is needed for the present numerical method. D'Humieres et al [3] analysed an electrical analogue of the present forced pendulum motion, giving particular attention to chaotic motion and the routes to chaos. Their choice of the value 1/8 for the damping ratio δ is adopted in the present calculations.

We describe those phase-locked solutions of (1.1) for which

$$\theta(t + mT) = \theta(t) \quad (T \equiv 2\pi/\omega), \tag{1.2a}$$

where m is the smallest integer for which (1.2a) is satisfied, as mT-periodic. When

$$\theta(t + mT/2) = -\theta(t), \tag{1.2b}$$

we describe the oscillation as symmetric. If $\langle\dot\theta\rangle/\omega$ is a rational number, ($\langle\rangle$ signifies a temporal average) and $\dot\theta$ is periodic, we describe the oscillation as running. (The adjective swinging may be applied to any oscillation for which $\langle\dot\theta\rangle = 0$, but is redundant for periodic oscillations.) Resonance curves are defined as plots of $\langle E\rangle^{\frac{1}{2}}$ vs ω, where

$$E = \dot\theta^2/2 + 1 - \cos\theta \tag{1.3}$$

is a measure of the energy of oscillation. Stability is determined through the numerical integration of (1.1) with initial conditions close to those of the solution to be tested.

We consider subsequently ([1], [2]) the coplanar oscillations of a weakly damped pendulum driven by horizontal and by vertical forcing of the pivot. The three cases are representative of the different types of forcing that can occur, given that linear superposition is not applicable. Strongly nonlinear effects, such as wave breaking on an oscillating fluid in a tank, are not modelled by the pendulum. Conversely, only some of the types of forced pendulum oscillation described here are possible in any particular mechanical system.

We obtain periodic solutions of (1.1) numerically by collocation applied to truncated Fourier expansions for $\theta(t)$. Considering, for example,

$$\theta = \sum_{k=0}^{N}(a_k \cos k\omega t + b_k \sin k\omega t), \tag{1.4}$$

and substituting into (1.1), we place the result in the form

$$F = \sum_{l=0}^{N}(F_l \cos l\omega t + G_l \sin l\omega t) = 0, \tag{1.5}$$

where the F_l, G_l are functionals of the a_k, b_k. The object is to choose the a_k, b_k so that the coefficients F_l, G_l are smaller than some prescribed error (typically 10^{-4}.) By differentiating F with respect to a_k, b_k in turn, followed by Fourier analysis of each partial derivative, the Jacobian for F_l, G_l with respect to a_k, b_k may be set up numerically. Trial values are taken for the a_k, b_k and are improved by Newton's method in Fourier space, using the Jacobian. The method is equivalent to collocation on an array of points equally spaced over one period of F. If the Fourier series (1.4), (1.5) are truncated at N harmonics, the accuracy of the expansion may be tested immediately by examining F_l, G_l for $l > N$. The number of harmonics, N, is increased until the residual harmonics, for $l > N$, are smaller than the prescribed error.

In addition, a systematic numerical search was made of the asymptotic solutions in time of (1.1), using step-by-step integration with the IMSL subroutine Dgear. It is a variable-step, variable-order Adams method, operated with a local error tolerance of 10^{-10}. Properties of the different forms of periodic solutions of (1.1), such as regions of occurrence, were calculated by the Fourier series method described above. The chaotic solutions of (1.1) were not investigated further, since our primary focus is on the bifurcation structure.

When the sinusoidal restoring force in (1.1) is replaced by the first two terms of the sine series, a weakly damped form of the forced Duffing equation is obtained. Oscillatory solutions of this equation are found to be similar to those of (1.1) at small θ, as expected, but lack the variety and interest of solutions of (1.1) at larger θ [7]. Forbes [5] used a numerical method based on Fourier series to calculate the periodic solutions of the forced Duffing equation. Perturbation series for the Fourier coefficients were introduced, a step which is unnecessary when the successive approximation is based on the addition of further Fourier coefficients, as described above.

Symmetric swinging oscillations of the form $\theta = \alpha \sin(\omega t - \phi)$ are analysed in [6], with the results being presented in terms of resonance curves for small values of ε. Comparisons are presented here between the exact results from a full Fourier-series expansion of θ and those found previously with truncation at the first harmonic. An unexpected property discovered here is that the approximation of θ by the first harmonic alone is valid not only at small $\varepsilon (< 0.5)$, but also at large $\varepsilon (> 1.5)$, owing to the domination of θ by the first harmonic.

The analysis of [6] was extended in [8] to swinging oscillations symmetric about the upward vertical of the form $\theta = \pi + \alpha \sin(\omega t - \phi)$. Comparison with the exact results shows the same unexpected validity of this approximation at large values of α and ε.

An interesting property demonstrated here is that each of the different forms of pendulum oscillation occurs in bands in the (ω, ε) plane, with the stable oscillations in one band having amplitudes differing by multiples of about π from those in the other bands for the given form of oscillation. The structure is reminiscent of that of energy levels in wave mechanics. The bands are classified into two types, major and minor. The major bands contain oscillations that occur for a much lower driving torque than in the neighbouring minor bands, for example an oscillation with a zero mean extending up to an amplitude near but before the upward vertical. The minor bands contain oscillations needing a much higher driving torque than in the neighbouring major bands, for example an oscillation with a zero mean extending up to and over the upward vertical, stopped by the torque at an amplitude near but before the next downward vertical. This minor band contains oscillations with amplitudes about π greater than the larger of the oscillations in the previous major band. Continuing these examples, the next major band contains oscillations with a zero mean, with the motion passing through the upward vertical and on through the downward vertical, with an amplitude near but before the next upward vertical. Oscillations in this major band have an amplitude about 2π greater than the larger of the oscillations in the previous major band. The major bands are broader than the minor bands on the (ω, ε) plane, with greater margins of stability.

2. T-periodic downward oscillations and their descendants

We represent T-periodic solutions of (1.1) by the Fourier series (1.4) where $a_0, \ldots, b_N$ and N are determined numerically, and $T \equiv 2\pi/\omega$. Symmetric, downward oscillations $[\theta(t + T/2) = -\theta(t)]$ are obtained by setting $a_{2j} = b_{2j} = 0$ $(j = 0, 1, 2, \ldots)$.

2.1. Symmetric oscillations

The resonance curve for symmetric oscillations with $\delta = 1/8$ and $\varepsilon = 0.4$ is plotted in Figure 1a. The lower part of the curve is triple valued in $\langle E \rangle^{\frac{1}{2}}$ between the two turning points $\omega = (\omega_-)_2 = 0.657$ and $\omega = \omega_+ = 0.750$, and the symmetric oscillations are unstable on the dotted section of the curve joining these points. The separate upper part of the curve in Figure 1a describes stable symmetric oscillations on the solid section between the

turning point at $\omega = (\omega_-)_1 = 0.538$ and the symmetry-breaking bifurcation point at $\omega = 0.470$ and unstable oscillations elsewhere. The value $\varepsilon = 0.4$ is slightly less than the maximum value $\varepsilon_\times$ (in the notation of [6]) for which the resonance curve separates into two parts, with $\varepsilon_\times = 0.403$ when $\delta = 1/8$. A comparison of the two solutions for stable symmetric oscillation at $\omega = 0.5$ shows that the oscillation on the lower part has an amplitude 0.17π, while that on the upper part has an amplitude 0.89π (almost to the upward vertical). A similar comparison at $\omega = 0.7$ finds an amplitude 0.28π on the lower stable section and 0.70π on the upper stable section. The resonance curve for symmetric oscillations at this value of ε calculated from [6], (3.2) and (3.11) lies on the top of the lower part to the accuracy of Figure 1a and differs only on the upper part, where the neglect of higher odd harmonics in [6] becomes significant.
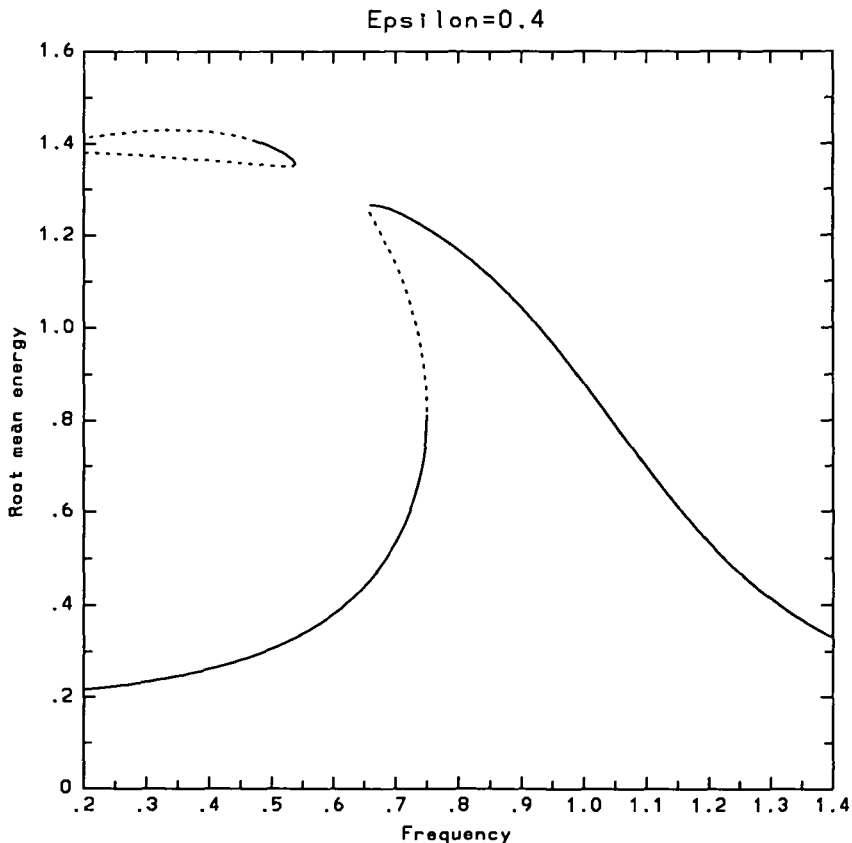
FIGURE 1a. The resonance curve for symmetric oscillations with $\varepsilon = 0.4$, $\delta = 1/8$. The oscillations are stable on the solid sections and unstable on the dotted sections.

When ε is increased from the value 0.4 of Figure 1a, the two parts join together. The lower section describes stable symmetric oscillations at all values of ω up to the right turning point at ω_+, and the upper section at all values of ω greater than the symmetry-breaking bifurcation value. An example of such a resonance curve at $\varepsilon = 0, 5$, $\delta = 1/8$ is given in [6], Figure 4, together with the approximate analytical curve for comparison.

As ε is increased further, the value ω_+ of the right turning point decreases, until the lower left section of the resonance curve is extinguished. Simultaneously, loops begin to form on the upper section of the resonance curve. The resonance curve at $\varepsilon = 1.2$, $\delta = 1/8$ is plotted in Figure 1b. Stable symmetric oscillations are described by the curve for all values of ω greater than the symmetry-breaking bifurcation value at $\omega = 0.870$. The solutions are unstable as ω continues along the resonance curve from this point until the upper right of the first loop is reached, where the symmetric oscillations are stable from the right turning point at $\omega = 0.403$ to a symmetry-breaking bifurcation point at $\omega = 0.390$. Another smaller interval of stability occurs at the upper right of the next loop, from the right turning point at $\omega = 0.268$ to a symmetry-breaking bifurcation point at $\omega = 0.264$, followed by a further smaller stable interval at the top of the third loop (not visible in Figure 1b), from the right turning point at $\omega = 0.205$ to a symmetry-breaking bifurcation point at $\omega = 0.203$. There is also a symmetry-breaking bifurcation point at $\omega = 0.209$, close to the left turning point at the lower left of the first loop, but the symmetric and asymmetric oscillations near this point are both unstable.

In the first stable interval of Figure 1b, spanning all values of ω greater than the first symmetry-breaking bifurcation value, the amplitude of the symmetric oscillations ranges from near zero at large ω to 0.82π at the bifurcation point. The range of amplitudes in the second stable interval is 2.61π to 2.80π, it is 4.69π to 4.84π in the third stable interval, and 6.66π to 6.76π in the fourth stable interval. In other words, symmetric oscillations in the first stable interval do not reach the upward vertical, those in the second stable interval pass through the upward vertical once in each direction during each forcing period with an amplitude near but before the next upward vertical, those in the third stable interval pass through the upward vertical twice consecutively in each direction during each forcing period with an amplitude near but before the next upward vertical, and so on.

The number of loops on the resonance curve increases as ε is increased from the value 1.2 of Figure 1b. The resonance curve at $\varepsilon = 2.0$, $\delta = 1/8$, is sketched in Figure 1c. The dominant, stable interval is bounded below by the symmetry-breaking value $\omega = 1.057$. Subsequent, major stable intervals, of decreasing width, are bounded above by the right turning points and below by
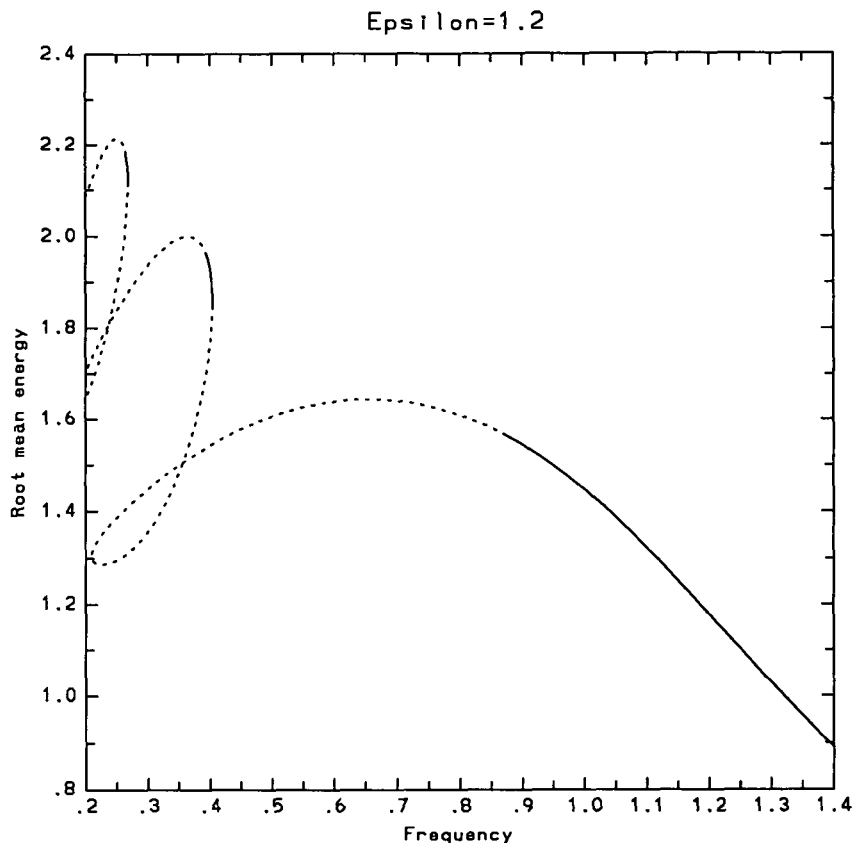
FIGURE 1b. The resonance curve for symmetric oscillations with $\varepsilon = 1.2$, $\delta = 1/8$. The oscillations are stable on the solid sections and unstable on the dotted sections.

symmetry-breaking bifurcation points on each loop of the resonance curve. The amplitude of the symmetric oscillations increases by 2π approximately between each of the consecutive stable intervals, as in the previous example.

A minor stable interval occurs at the first left turning point (magnified in the inset to Figure 1c), from a symmetry-breaking bifurcation value at $\omega = 0.4521$ to the turning point at $\omega = 0.4505$. Stable symmetric oscillations in this interval have amplitudes in the range 1.69π to 1.71π, differing by about π from amplitudes in the major stable intervals on either side. The margin of stability in this region is small, which is to be expected when the amplitude lies near the downward vertical for an oscillation passing through the upward vertical. Oscillations in this interval are unstable in Figure 1b at $\varepsilon = 1.2$, but the larger driving force ($\varepsilon = 2.0$) in Figure 1c is sufficient to stabilise this unusual motion. A smaller stable interval occurs at the second left turning
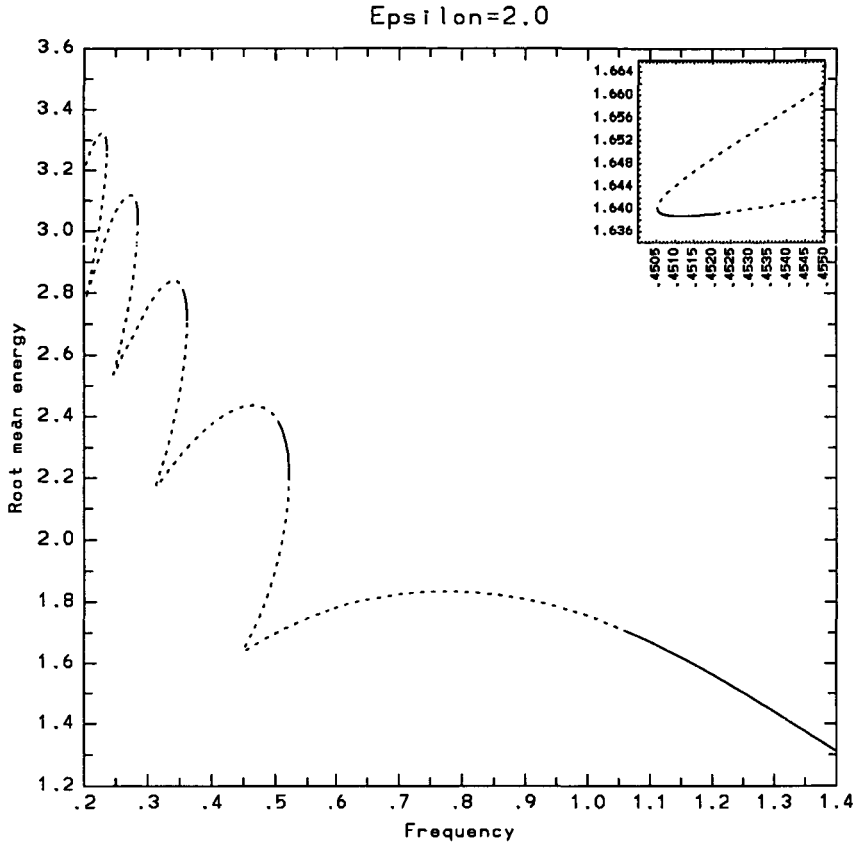
FIGURE 1c. The resonance curve for symmetric oscillations with $\varepsilon = 2.0$, $\delta = 1/8$. The oscillations are stable on the solid sections and unstable on the dotted sections. The first left turning point is magnified in the inset.

point, where $\omega = 0.313$, with an amplitude 3.69π. Symmetry-breaking bifurcation points occur near the third and fourth left turning points, but the motions near these points are unstable at $\varepsilon = 2.0$.

The resonance curve from Figure 1c is compared in Figure 1d with the approximate analytical resonance curve obtained from [6], (3.2) and (3.11),

$$\omega^2 = \Omega - 2\delta^2 \pm (\varepsilon^2/\alpha^2 - 4\delta^2\Omega + 4\delta^4)^{\frac{1}{2}} \tag{2.1a}$$

and

$$\langle E \rangle^{\frac{1}{2}} = \left(\alpha^2\omega^2/4 + 1 - J_0(\alpha)\right)^{\frac{1}{2}} \tag{2.1b}$$

where $\Omega = -2\alpha^{-1}J_0'(\alpha)$. This excellent agreement was unexpected, because θ is approximated by the first harmonic alone in these calculations. However, a full Fourier expansion of θ (with all even harmonics zero) shows that
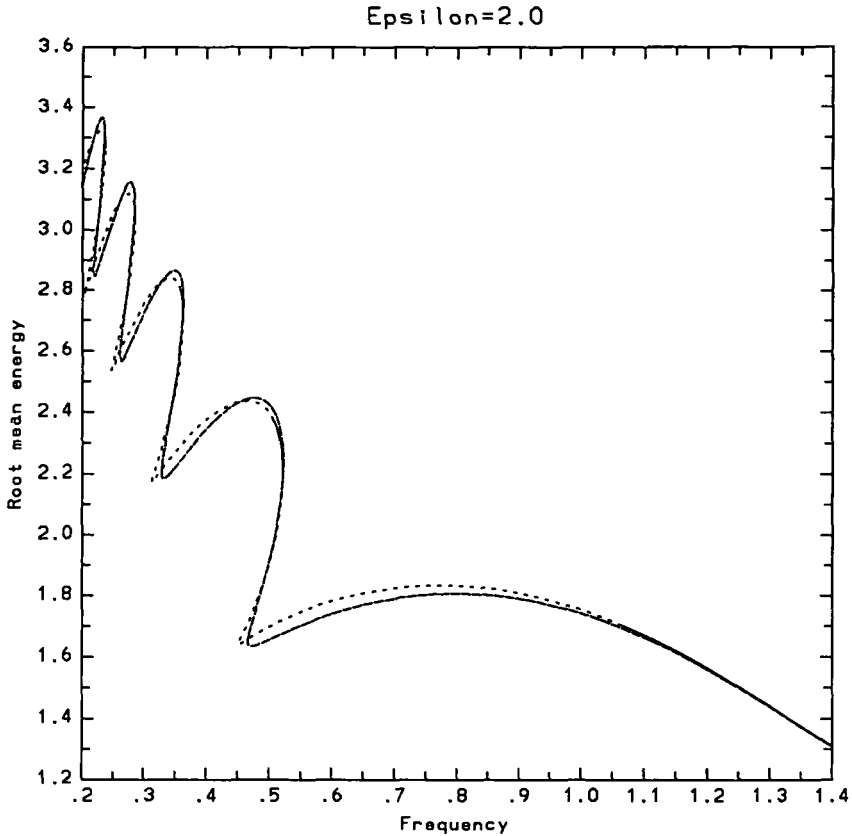
FIGURE 1d. The resonance curve from Figure 1c, with the dashed approximate analytical curve (2.1).

it is dominated by the first harmonic at these larger values of ε and α. For Figures 1c, 1d, the ratio of the third to the first harmonics is 0.017 at the first major bifurcation point $\omega = 1.057$, 0.020 at the third major bifurcation point $\omega = 0.356$ and 0.018 at the fifth major bifurcation point $\omega = 0.235$. (The major bifurcation points, after the first, bound the major stable intervals extending to each of the right turning points.) We note that, at the fifth major bifurcation point, the first harmonic has a magnitude (α in the analytical approximation) 8.53π, where the stable symmetric oscillation has an amplitude 8.75π.

The ratio of the third to the first harmonics is larger at the minor bifurcation points (near the left turning points). At the first minor bifurcation point, $\omega = 0.452$, the ratio is 0.042, and at the second minor bifurcation point, $\omega = 0.313$, it is 0.045. The larger value of this ratio is consistent

with the lesser accuracy in Figure 1d of the analytical approximation at the left turning points.

The symmetric oscillations approximated in [6] by $\theta = \alpha \sin(\omega t - \phi)$ are shown there to follow the resonance curve given by (2.1). The asymptotic form for the J_0 Bessel function is

$$J_0(\alpha) = \left(\frac{2}{\pi\alpha}\right)^{\frac{1}{2}} \cos\left(\alpha - \frac{1}{4}\pi\right) + O\left(\frac{1}{\alpha}\right). \qquad (2.2)$$

It follows that, for given ε and δ, at large α, $\langle E \rangle^{\frac{1}{2}}$ exhibits a similarity in form with a periodicity of 2π in α. This similarity is evident in Figures 1b, c, d and is consistent with the amplitudes in major and minor stable intervals differing by multiples of π.

2.2. Asymmetric oscillations

Asymmetric, T-periodic oscillations are represented here by the full Fourier series (1.4) and in [6] by $\theta = \theta_0 + \alpha \sin(\omega t - \phi)$, $-\pi < \theta_0 \leq \pi$, $\alpha > 0$, $0 \leq \phi \leq \pi$. The symmetry-breaking boundary between symmetric and asymmetric oscillations is determined numerically by calculating the curve on which the even harmonics of the asymmetric oscillations tend to zero, and in the approximate model by allowing θ_0 to tend to zero. It is the stability boundary for the symmetric oscillations, with symmetric oscillations on the unstable side of the curve losing stability to asymmetric oscillations.

It is shown in [6], (2.2a), that symmetry-breaking occurs when $J_0(\alpha) = 0$, where it was assumed that only the first zero of J_0 is relevant. However, the above analysis suggests that the higher zeros of J_0 also are relevant. The symmetry-breaking curves, adapting [6], (4.1a, b), then are

$$\varepsilon^2 = \alpha_n^2(\omega^2 - \Omega_n + 2\delta^2)^2 + 4\delta^2\alpha_n^2(\Omega_n - \delta^2), \qquad (2.3)$$

$n = 1, 2, \ldots$, where α_n is the nth zero of J_0, and $\Omega_n = -2\alpha_n^{-1}J_0'(\alpha_n)$. The exact major, symmetry-breaking curves, calculated numerically from (1.4), are compared in Figure 2 with the approximate major curves given by (2.3) with $n = 1, 3, 5, 7, 9$. Although the analytical approximation is unsatisfactory for the first symmetry-breaking curve, the agreement is excellent for the higher curves in that (2.3) does predict the major symmetry-breaking curves accurately for the larger odd values of n.

The minor symmetry-breaking curves, near the left turning points in Figures 1b, c,d are approximated by the even values of n in (2.3). It can be seen in Figure 1d that the analytical approximation does not provide an accurate estimate of the left turning points. This inaccuracy is reflected in an unsatisfactory fit between the approximate and exact minor symmetry-breaking
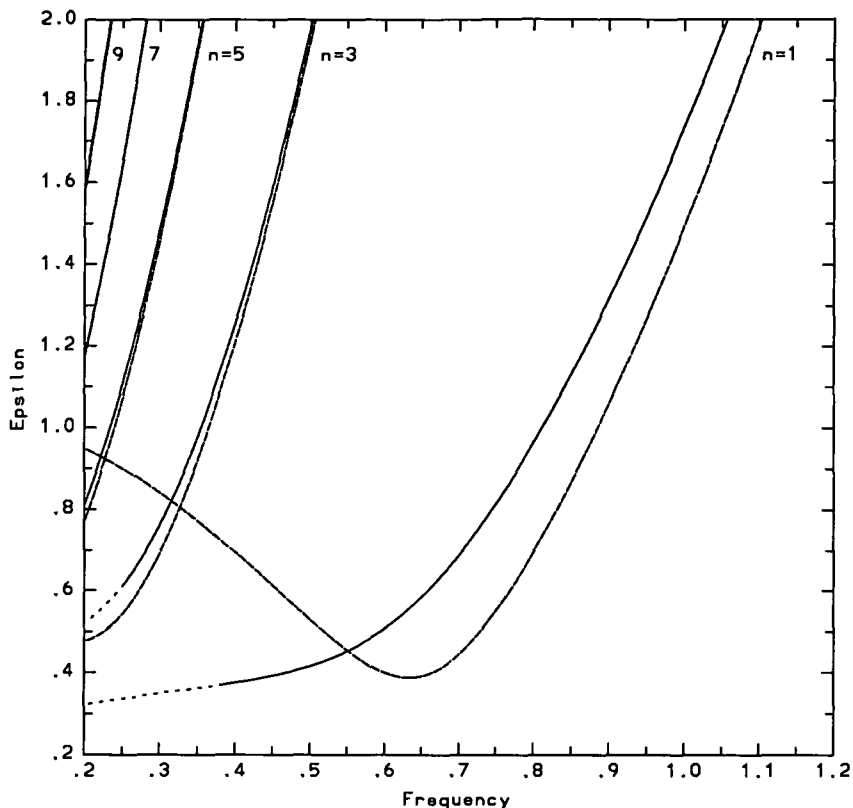
FIGURE 2. The symmetry-breaking curves for oscillations with $\delta = 1/8$. The solid and dotted curves are the numerically calculated results, and the dashed curves are the approximate results (2.3) with the values of n shown.

curves, which proves to be qualitative only, without the quantitative accuracy of Figure 2.

As ω is changed further at fixed ε, the T-periodic, asymmetric oscillations become unstable in turn, tending asymptotically in time to $2T$-periodic, asymmetric oscillations. This period-doubling sequence continues to $4T$, $8T$, ... -periodic, asymmetric oscillations. The mT-periodic asymmetric oscillations are calculated using the Fourier expansion

$$\theta = \sum_{k=0}^{N}[a_k \cos(k\omega t/m) + b_k \sin(k\omega t/m)], \qquad (2.4)$$

where $a_0, \ldots, b_N$ and N are determined numerically. The bifurcating resonance curves are illustrated in [6], Figure 5, for $\varepsilon = 0.5$, $\delta = 1/8$. Here, in Figure 3, the pattern of bifurcation is sketched for $\varepsilon = 2.0$, $\delta = 1/8$. The
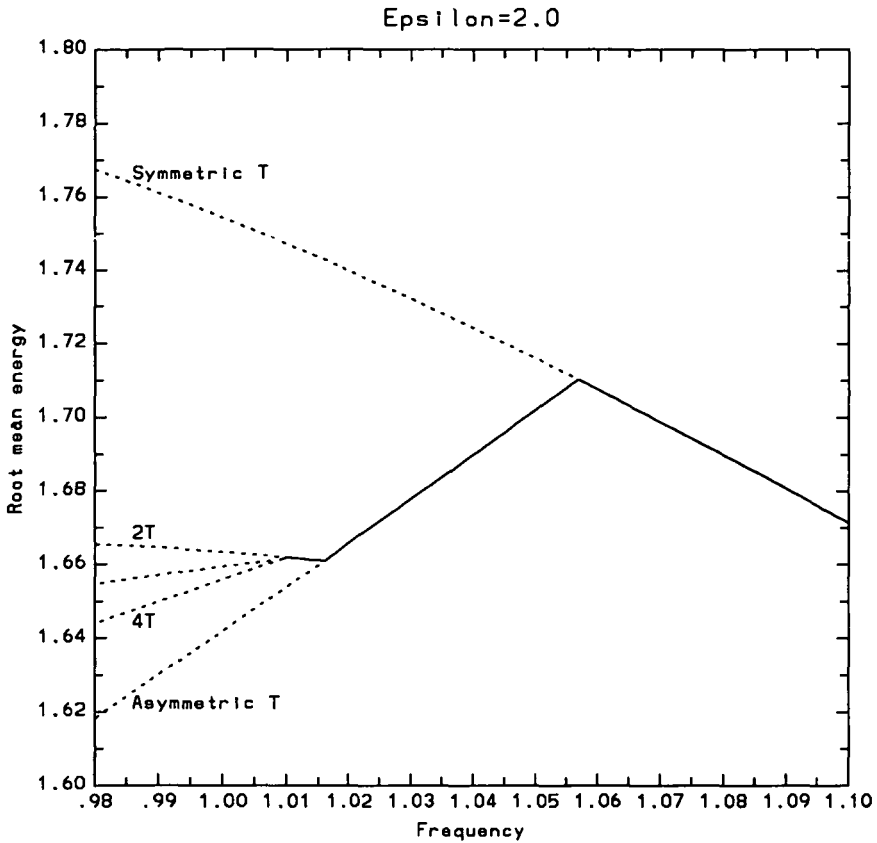
FIGURE 3. Resonance curves for the symmetry-breaking, period-doubling sequence of periods T, $2T$, $4T$, ... , with $\varepsilon = 2.0$, $\delta = 1/8$. The oscillations are stable on the solid sections and unstable on the dotted sections.

symmetry-breaking, period-doubling sequence is shown by the stable (solid) resonance curves, with the unstable (dotted) continuations sketched also. The resonance curves leap-frog towards the unlabelled curve for $8T$-periodic oscillations. The $16T$-periodic curve is slightly below the $8T$-periodic curve, but is indistinguishable from it on the scale of the figure. The pattern in Figure 3 at $\varepsilon = 2.0$ is the same as that in [6], Figure 5 at $\varepsilon = 0.5$, but on the same scale it is found that the angles and curve lengths all differ. The ratios of the curve lengths approximate those predicted by Feigenbaum [4], but cannot be compared exactly because the ratios depend on ε as well as ω, while Feigenbaum's analysis is applied to one-parameter problems.

The symmetry-breaking, period-doubling sequence illustrated by resonance curves in Figure 3 is demonstrated alternatively by the stable $(\theta, \dot{\theta})$ phase-
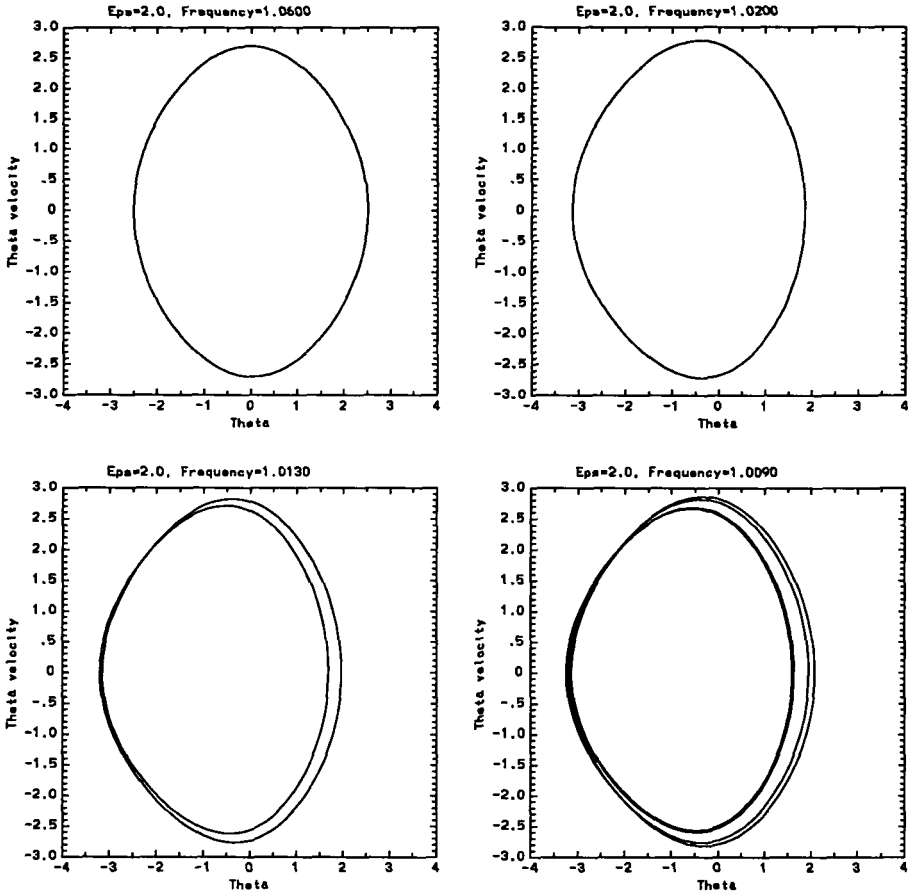
FIGURE 4. $(\theta, \dot{\theta})$ phase-plane orbits for the symmetry-breaking, period-doubling sequence of periods T, $2T$, $4T$ with $\varepsilon = 2.0$, $\delta = 1/8$.

plane orbits in Figure 4. The first orbit, at $\omega = 1.06$, is of a symmetric T-periodic oscillation with an amplitude $2.509(= 0.80\pi)$. Symmetry-breaking has occurred in the second orbit, at $\omega = 1.02$, the maximum and minimum angles θ being $1.858(= 0.59\pi)$ and $-3.135(= -0.998\pi)$. The amplitude of the oscillation is almost the same as in the symmetric orbit, but the mean has moved to -0.20π. The third orbit, at $\omega = 1.013$, illustrates period-doubling to a $2T$-periodic oscillation, and the fourth orbit, at $\omega = 1.009$, shows further periodic-doubling to a $4T$-periodic oscillation. The minimum angles θ in the third and fourth orbits are $-3.203(= -1.02\pi)$ and $-3.247(= -1.03\pi)$ respectively. The angles are of this magnitude (slightly past the upward vertical) because the driving force is large, the maximum driving acceleration being $2g(= \varepsilon g)$.
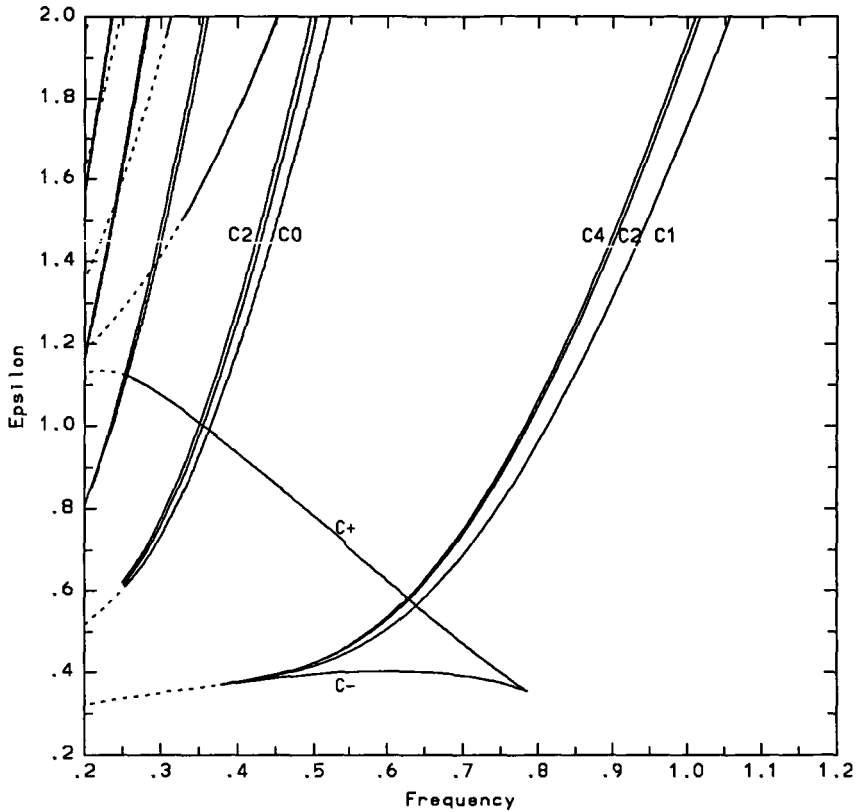
FIGURE 5. Stability boundaries for oscillations of periods T, $2T$, $4T$, with $\delta = 1/8$. C_-, C_+, C_0 are turning point curves, C_1 is a symmetry-breaking curve, and C_2, C_4 are period-doubling curves.

The stability boundaries for swinging oscillations of periods T, $2T$, and $4T$ are summarised in Figure 5. The C_+ curve is the locus of the lower turning point ω_+, when this occurs, as in Figure 1a. It marks the stability boundary for stable symmetric oscillations at small ω and $\langle E \rangle^{\frac{1}{2}}$. The section of the resonance curves describing these oscillations is extinguished at about $\varepsilon = 1.13$ (for $\delta = 1/8$). The C_- curve is the locus of the upper turning point(s), when they occur. There are two upper turning points, ω_- in Figure 1a, corresponding to the two intersections of the line $\varepsilon = 0.4$ with the C_- curve. The right curve C_1 is the first major symmetry-breaking curve from Figure 2. Stable symmetric oscillations are found everywhere between, and to the right of, the C_- curve and the right C_1 curve. Independent, stable, symmetric oscillations are found everywhere to the left of the C_+ curve. The two families are the same for all ε below the intersection of the C_-

and C_+ curves. The two independent families exist together in the triangle between the C_-, C_+, and right C_1 curves (as in the examples for $\omega = 0.5$, $\omega = 0.7$ taken from Figure 1a). The dotted continuation of the C_- and right C_1 curves is the locus of the turning point on the upper part of the resonance curve, where it becomes difficult to find a stable oscillation. The analytically calculated C_+ and part of the C_- curves are sketched in [6], Figure 3. There is reasonable agreement between the analytical approximate C_+ and C_- curves and the numerically exact C_+ and C_- curves of Figure 5.

Stable, T-periodic, asymmetric oscillations occur in the band between the right C_1 and C_2 curves, where C_2 is the first period-doubling stability boundary, and stable, $2T$-periodic, asymmetric oscillations are found between the C_2 and C_4 curves. Period doubling occurs again on C_4, and stable, $4T$-periodic, asymmetric oscillations exist between C_4 and C_8 (the latter curve is not drawn in Figure 5 because it is indistinguishable from C_4 on the scale of the figure). As ω is decreased slightly from C_8, nearly-periodic oscillations occur with orbits near those in the period-doubling sequence. Although chaotic motion may ensue when ω is decreased again, in practice there are so many alternative stable solutions that the motion asymptotic in time is typically an independent family of oscillations. When the period-doubling sequence is followed through the right family of curves $C_2, C_4, \ldots$ at the larger values of ε in Figure 5, (as in Figures 3 and 4, for example) the motion tends asymptotically in time to a T-periodic running oscillation with a mean angular velocity ω for values of ω beyond the above period-doubling sequence.

The major bands of stable, T-periodic, oscillations after the first, corresponding to $n = 3, 5, 7, 9$ in (2.3), begin on the right of each band with a C_0 turning-point stability boundary. This is a sharp transition between stable, T-periodic, symmetric oscillations on the left and chaotic or some independent stable motion on the right of the curve. It is follows by a symmetry-breaking stability boundary, C_1 from Figure 2, and then by periodic-doubling stability boundaries $C_2, C_4, \ldots$. The dotted curve at the base of the $n = 3$ band denotes the section where it is difficult to find stable oscillations of fixed periodicity.

The minor bands of T-periodic oscillations correspond to $n = 2, 4, 6, 8$ in (2.3). The stable sections have a turning point boundary C_0 on the left of each band, followed by a symmetry-breaking boundary C_1 towards the right of the band. The period-doubling boundaries C_2 are indistinguishable from the C_1 boundaries on the scale of the figure. The dotted curves on the minor bands correspond to unstable oscillations.

3. T-periodic inverted oscillations and their descendants

We represent T-periodic, inverted solutions of (1.1) by the Fourier series

$$\theta = \theta_0 + \sum_{k=1}^{N}(a_k \cos k\omega t + b_k \sin k\omega t),\qquad(3.1)$$

where $\theta_0 = \pi$, $a_{2j} = b_{2j} = 0$, $j = 1, 2, \ldots$, for symmetric oscillations, and θ_0 lies near π with all harmonics present for asymmetric oscillations. Symmetric oscillations are investigated in [8] with the truncated form

$$\theta = \pi + \alpha \sin(\omega t - \phi).\qquad(3.2)$$

The resonance curves for symmetric, inverted oscillations display a similar looping structure to those of the downward oscillations at larger ε, with the number of loops increasing as ε increases. The lowest value of ε for which stable inverted solutions occur is about 0.48 (for $\delta = 1/8$), at which the resonance curve has one loop and the stable interval lies near the right turning point of the loop. The analytical approximation (3.2) is not accurate for this ε, the ratio of the third to the first harmonics being about 0.07. As ε is increased, this major band of stable symmetric inverted oscillations increases in width, being bounded on the right by the right turning-point curve and on the left by the first major symmetry-breaking curve. Further major, stable bands occur as further loops appear on the resonance curve, each being bounded on the right by a right turning-point curve and on the left by a major symmetry-breaking curve. Minor symmetry-breaking curves are found near left turning points, as for the downward oscillations, but the solutions near these points are unstable for ε less than about 1.31.

The resonance curve for inverted, symmetric, T-periodic oscillations at $\varepsilon = 2.0$ is sketched in Figure 6a. The first major stable interval extends from the right turning point at $\omega = 0.712$ to the symmetry-breaking bifurcation value $\omega = 0.656$, in which the symmetric oscillations have a mean of π and amplitudes between 1.44π at the turning point to 1.79π at the bifurcation point. The second major stable region on the second loop extends from the right turning point at $\omega = 0.424$ to the symmetry-breaking bifurcation value $\omega = 0.413$, with symmetric inverted oscillations having amplitudes between 3.65π and 3.81π, about 2π greater than those in the first major band. The next major band describes stable symmetric inverted oscillations with amplitudes near 5.65π, and the fourth major band with amplitudes near 7.65π.

The first minor stable region extends from the first left turning point at $\omega = 0.633$ to a symmetry-breaking bifurcation point at $\omega = 0.639$, with amplitudes in the range 0.75π to 0.70π respectively. This is the stable
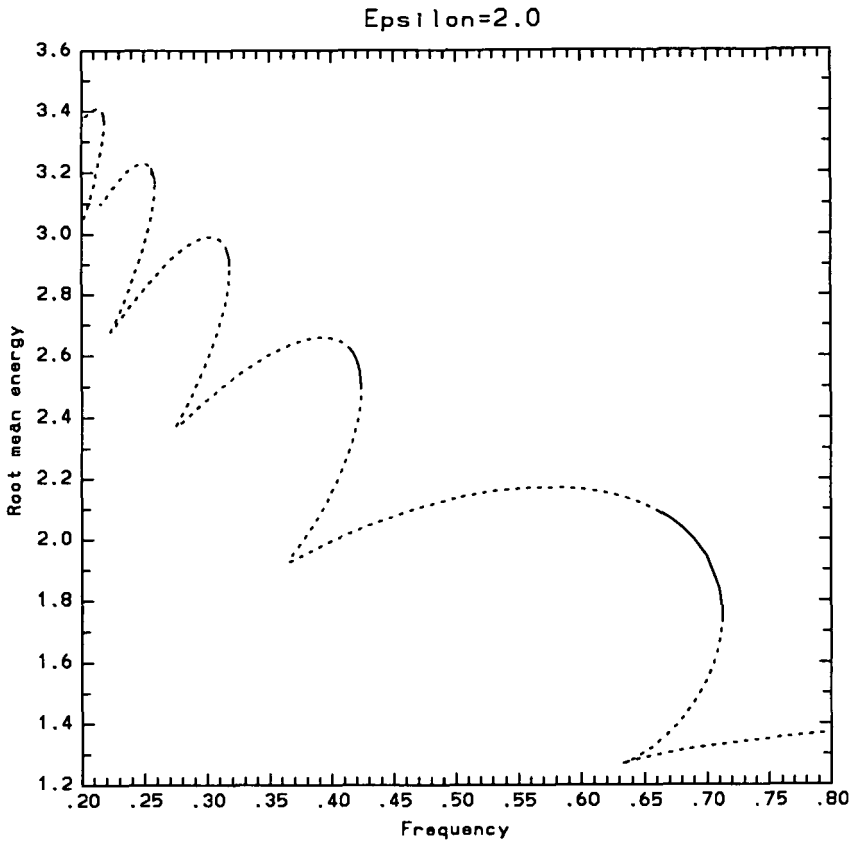
FIGURE 6a. The resonance curve for symmetric inverted oscillations with $\varepsilon = 2.0$, $\delta = 1/8$.
The oscillations are stable on the solid sections and unstable on the dotted sections.

interval identified in [8], where it had not been expected that the approximate representation (3.2) would be valid for larger values of α. The above values for ω and α agree with those describing the stable interval for $\varepsilon = 2.0$ in [8], Figure 1. The symmetric oscillations in this band are unusual, having the upward vertical as a mean, but being stopped by the torque before reaching the downward vertical. It is not surprising that the torque must be large ($\varepsilon >$ 1.31) for the oscillations in this band to be stable. The second minor stable band occurs in the neighborhood of the left turning point at $\omega = 0.365$, with amplitudes near 2.71π, about 2π greater than those in the first minor band. Symmetric inverted oscillations in the third minor band near the left turning point $\omega = 0.275$ are also stable for $\varepsilon = 2.0$, with amplitudes near 4.68π, but those near the left turning point $\omega = 0.224$ are unstable for $\varepsilon = 2.0$.

The exact resonance curve for $\varepsilon = 2.0$, from Figure 6a, is compared in Figure 6b with the approximate analytical resonance curve, calculated from
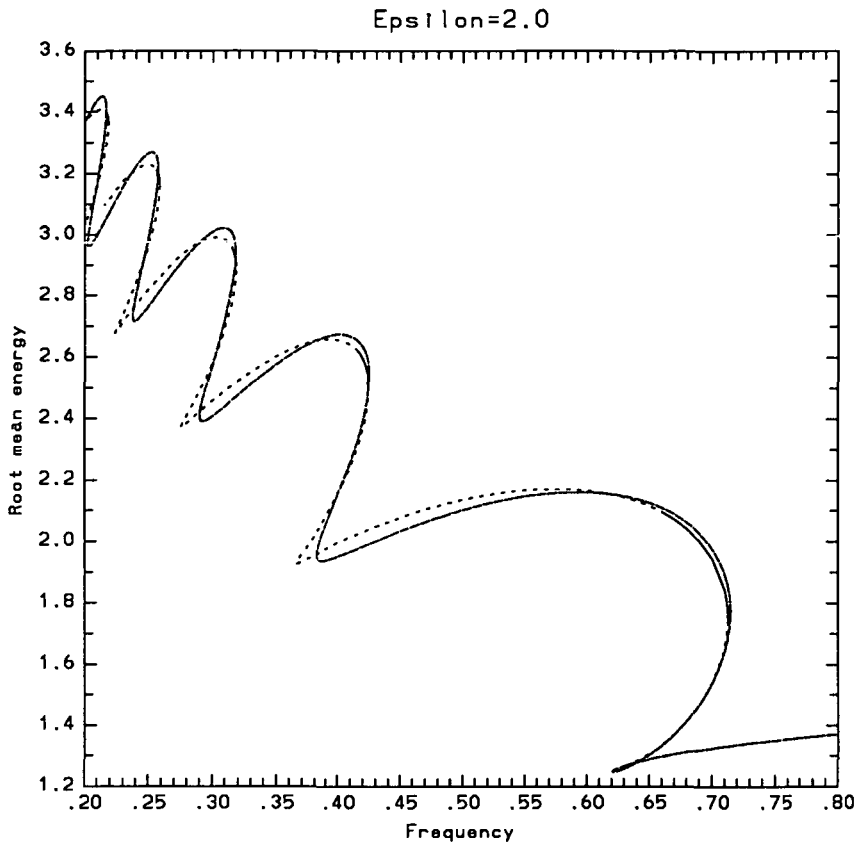
FIGURE 6b. The resonance curve from Figure 6a, with the dashed approximate analytical curve.

[8], (4a) with (1.3) above. The agreement is excellent, apart from the left turning points after the first. This close fit was unexpected because of the large amplitudes of oscillation, and it occurs for the same reason as for the downward oscillations, that the Fourier expansions for θ are dominated by the first harmonic. At the first major bifurcation point $\omega = 0.656$, the ratio of the third harmonic to the first harmonic is 0.023, while at the fourth major bifurcation point $\omega = 0.256$ (where the first harmonic has magnitude 7.58π) this ratio is only 0.018.

The stability boundaries for inverted oscillations of periods T and $2T$ are summarised in Figure 7. The major stability bands correspond to $n = 2, 4, 6, 8$ in (3.3), and the minor stability bands to $n = 1, 2, 5, 7$ in (3.3). (The oscillations in the n th band have amplitudes near to but less than $n\pi$).
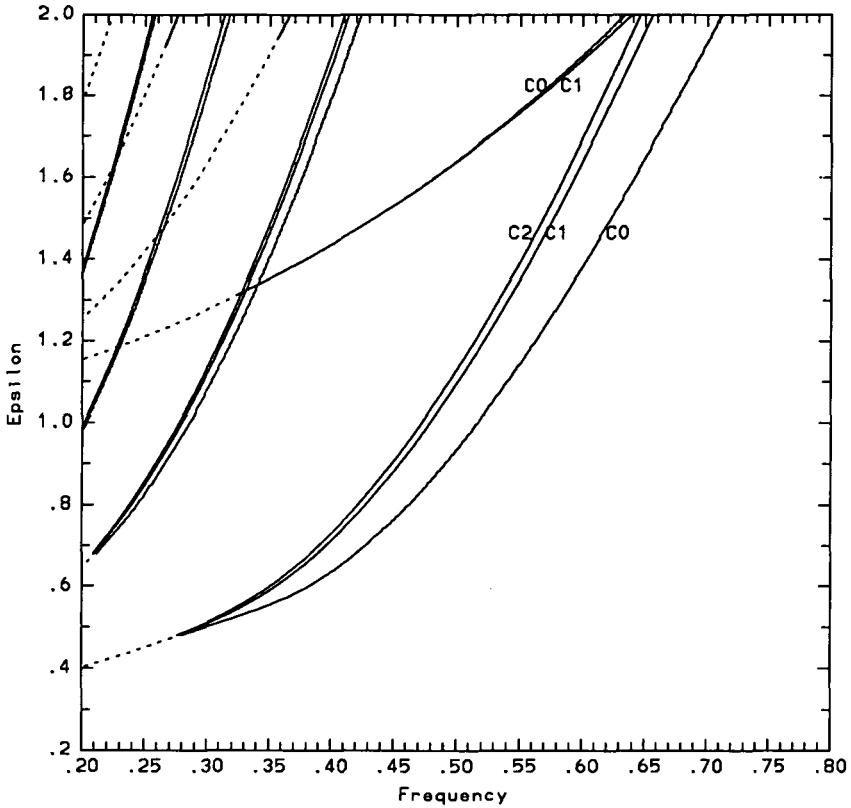
FIGURE 7. Stability boundaries for inverted oscillations of periods T, $2T$, with $\delta = 1/8$. C_0 denotes turning point curves, C_1 symmetry-breaking curves, and C_2 a period-doubling curve.

Each of the major bands is bounded on the right by a turning-point curve C_0, then progresses to the left through the symmetry-breaking curve C_1 and the period-doubling curves C_2, C_4, ... The sequence is reversed on each of the minor bands because they begin on left turning points. The first minor band, with the smallest amplitudes, is that described in [8]. The bands are dotted where the oscillations are unstable.

If θ is represented by the truncated form (3.2), symmetry breaking occurs when $J_0(\alpha) = 0$, for the reasons indicated in [6], (2.2a). It follows from [8], (3a, b) that the symmetry-breaking curves for inverted, T-periodic oscillations satisfy

$$\varepsilon^2 = \alpha_n^2(\omega^2 + \Omega_n + 2\delta^2)^2 - 4\delta^2\alpha_n^2(\Omega_n + \delta^2), \qquad (3.3)$$

$n = 1, 2, \ldots$, where α_n is the nth zero of J_0, and $\Omega_n = -2\alpha_n^{-1}J_0'(\alpha_n)$. The exact symmetry-breaking curves, calculated numerically from (3.1), are
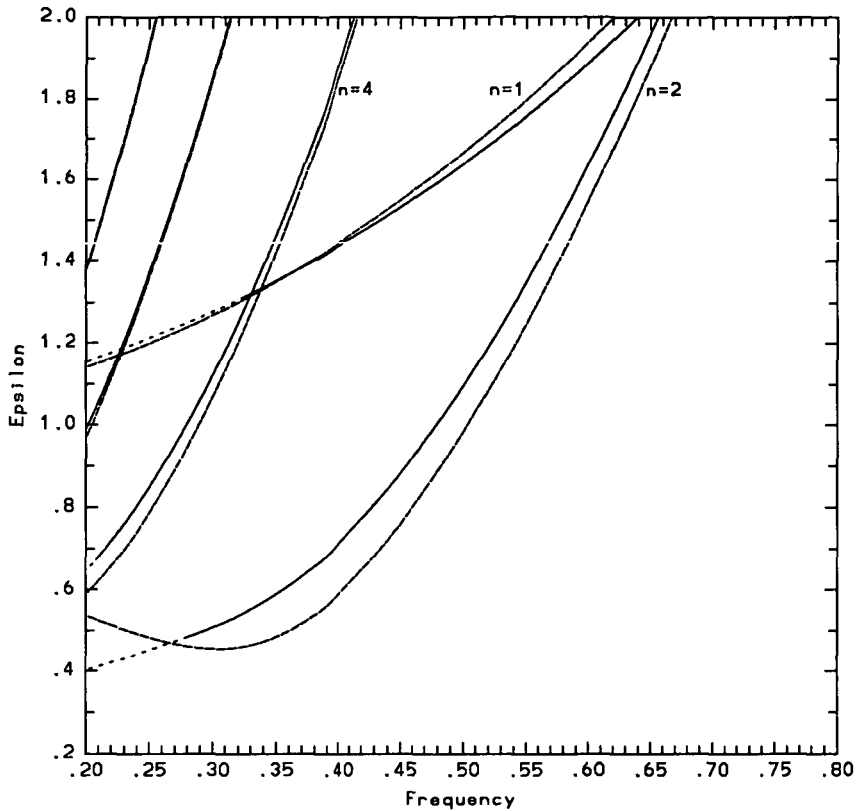
FIGURE 8. The symmetry-breaking curves for inverted oscillations with $\delta = 1/8$. The solid and dotted curves are the numerically calculated results, and the dashed curves are the approximate results (3.3) with the values of n shown.

compared in Figure 8 with the approximate curves given by (3.3) with $n = 1, 2, 4, 6, 8$. The even values of n describe the major symmetry-breaking curves, and $n = 1$ describes the first minor symmetry-breaking curve. The agreement is excellent for the higher major curves, and is satisfactory for the lower major curves and for the first minor curve. The higher minor curves are not drawn in Figure 8 because the fit between the exact and approximate curves is qualitative only, which is anticipated by the lack of accuracy at the left turning points in Figure 6b.

4. Further stable oscillations

The torque-driven pendulum has a full range of stable oscillatory solutions, including oscillations of periods $3T$, $5T$, $7T$, ..., both symmetric

or asymmetric, downward or inverted, and their descendants. Systematic integration of (1.1) for a range of values of ε and ω shows the same banded stability structure for these other forms of oscillatory solution of (1.1) as is described above for T-periodic solutions and their descendants.

An example is provided by running oscillations with mean angular velocity ω, described by

$$\theta = \omega t + \sum_{k=0}^{N} [a_k \cos k\omega t + b_k \sin k\omega t]. \tag{4.1}$$

The oscillations relative to the mean rotation ωt are asymmetric and T-periodic. When $\varepsilon = 2.0$, the oscillations relative to the mean rotation in the first dominant stable band have amplitudes between 0.48π and 0.81π with means of about 0.05π. The relative amplitudes in the second stable band lie near 1.92π, with means of about 0.05π also. In other words, the amplitudes of the asymmetric motion relative to the mean rotation increase by about π between consecutive stable bands. However, the next stable band when $\varepsilon = 2.0$ has almost the same relative amplitudes as the previous stable band, but it has relative means that lie near π. The running oscillations in this stable band are inverted asymmetric oscillations relative to the mean rotation. This pattern continues in subsequent stable bands, with increases of about π in the amplitudes between bands whose means relative to ωt lie near zero, and independently, increases of about π in the amplitudes between bands whose means relative to ωt lie near π.

The banded stability structure appears to be an intrinsic property of the torque-driven pendulum, and it has not yet been found for other forced pendulums.

Acknowledgements

References

[1] Peter J. Bryant and John W. Miles, "On a periodically-forced, weakly damped pendulum. Part 2: Horizontal forcing", *J. Austral. Math. Soc. Ser B*. **32** (1990) 23–41.

[2] Peter J. Bryant and John W. Miles, "On a periodically-forced, weakly damped pendulum. Part 3: Vertical forcing", *J. Austral. Math. Soc. Ser. B*. **32** (1990) 42–60.

[3] D. D'Humieres, M. R. Beasley, B. A. Huberman and A. Libchaber, "Chaotic states and routes to chaos in the forced pendulum", *Phys. Rev. A* **26** (1982) 3483–3496.

[4] Mitchell J. Feigenbaum, "Quantitative universality for a class of nonlinear transformations", *J. Stat. Phys.* **19** (1978), 25–52.

[5] Lawrence K. Forbes, "Periodic solutions of high accuracy to the forced Duffing equation: Perturbation series in the forcing amplitude", *J. Austral. Math. Soc. Ser. B* **29** (1987) 21–38.

[6] John Miles, "Resonance and symmetric breaking for the pendulum", *Physica D* **31** (1988) 252–268.

[7] John Miles, "Resonance and symmetry breaking for a Duffing oscillator", *SIAM J. Appl. Math.* **49** (1989) 968–981.

[8] John Miles, "Directly forced oscillations of an inverted pendulum", *Phys. Lett. A.* **133** (1988) 295–297.